Friction **12**(6): 1299–1321 (2024)
https://doi.org/10.1007/s40544-023-0834-7
ISSN 2223-7690
CN 10-1237/TH
RESEARCH ARTICLE

Predicting the coefficient of friction in a sliding contact by applying machine learning to acoustic emission data

Robert GUTIERREZ[1,*], Tianshi FANG[2], Robert MAINWARING[3], Tom REDDYHOFF[1,*]

[1] *Tribology Group, Department of Mechanical Engineering, Imperial College London, Exhibition Road, London SW7 2AZ, UK*

[2] *Shell Global Solutions (US) Inc. Shell Technology Center Houston, 3333 Highway 6 South, Houston, TX 77082, USA*

[3] *Shell International Petroleum Company Limited, Shell Centre, York Road, London SE1 7NA, UK*

Received: 28 April 2023 / Revised: 28 June 2023 / Accepted: 21 September 2023

Abstract: It is increasingly important to monitor sliding interfaces within machines, since this is where both energy is lost, and failures occur. Acoustic emission (AE) techniques offer a way to monitor contacts remotely without requiring transparent or electrically conductive materials. However, acoustic data from sliding contacts is notoriously complex and difficult to interpret. Herein, we simultaneously measure coefficient of friction (with a conventional force transducer) and acoustic emission (with a piezoelectric sensor and high acquisition rate digitizer) produced by a steel–steel rubbing contact. Acquired data is then used to train machine learning (ML) algorithms (e.g., Gaussian process regression (GPR) and support vector machine (SVM)) to correlated acoustic emission with friction. ML training requires the dense AE data to first be reduced in size and a range of processing techniques are assessed for this (e.g., down-sampling, averaging, fast Fourier transforms (FFTs), histograms). Next, fresh, unseen AE data is given to the trained model and the resulting friction predictions are compared with the directly measured friction. There is excellent agreement between the measured and predicted friction when the GPR model is used on AE histogram data, with root mean square (RMS) errors as low as 0.03 and Pearson correlation coefficients reaching 0.8. Moreover, predictions remain accurate despite changes in test conditions such as normal load, reciprocating frequency, and stroke length. This paves the way for remote, acoustic measurements of friction in inaccessible locations within machinery to increase mechanical efficiency and avoid costly failure/needless maintenance.

Keywords: acoustic emission; condition monitoring; friction; machine learning; Gaussian process regression; support vector machine

1 Introduction

Sliding components such as gears, clutch discs, and mechanical seals are common in machinery across many industries. These parts are a source of friction and wear, both of which contribute to large economic losses as friction reduces machine efficiency and worn parts must be maintained and replaced. It is estimated that 20% of global energy consumption is spent overcoming friction [1, 2]. Being able to measure friction in sliding components within machines would enable efficiency to be monitored and improved by applying control strategies. This would allow costly failures and needless maintenance to be avoided. In fact, the machine condition monitoring market is estimated to grow to 3.5 billion US$ by 2024 [3]. More specifically, the monitoring of oil quality in machines such as engines, gear-systems and turbines across oil and gas, transportation, and manufacturing industries is estimated to increase by 6.1% by 2026, reaching 1.4 billion US$ [4].

A promising method of monitoring tribological

* Corresponding authors: Robert GUTIERREZ, E-mail: robert.gutierrez16@imperial.ac.uk; Tom REDDYHOFF, E-mail: t.reddyhoff@imperial.ac.uk

contacts is to analyse the elastic mechanical stress waves, which propagate through a material due to sudden releases of energy [5, 6]. This is known as acoustic emission (AE) and is already widely used as a non-destructive testing method to monitor rail failure [7], steel tanks [8], gear tooth fatigue [9], and the formation, development, and location of cracks [10–13]. AE is typically recorded as a voltage from a piezoelectric transducer coupled to a sliding component in the vicinity of the interface. Specifically for sliding contacts, Sun et al. [14] identified possible sources of acoustic emission as contact surface damage, subsurface crack formation, impulsive shocks from asperity collisions and material phase changes. A more detailed evidence-based understanding of AE mechanisms is still lacking, despite AE data being believed to be a rich source of tribological information [15–17].

Compared to other common techniques, AE monitoring of sliding contacts has the advantage of working remotely without contacting the interface. Furthermore, AE requires neither a transparent window (as with optical techniques) [18] nor conductive materials (as with electrical techniques) [19, 20]. As a result, there have been many attempts to find correlations between AE and tribological parameters. Early studies focused on time-based parameters such as AE RMS used by Miettinen and Siekkinen [15] to quantify leakage in mechanical seals. Jiaa and Dornfeld [21] identified running in, steady state, and self-acceleration wear regions in their AE RMS signal. A relation between cumulative AE counts (number of points above a threshold) and frictional work done was proposed by Lingard and Ng [16]. There have also been some empirical models relating wear to acoustic emission, such as a power law relating the integrated RMS signal to wear volume proposed by Boness et al. [17]. Subsequent studies attempted to develop a theoretical basis for AE, e.g., by using elastic asperity contact modelling to relate AE RMS to sliding speed and normal load for an assumed probability distribution for contacting asperities [22]. This model was further developed by Hu et al. [23], who proposed a bi-Gaussian distribution for asperity heights, and by Towsyfan et al. [24] who modelled asperity interactions with beam theory and derived equations for AE RMS produced from asperity-fluid interactions. A limitation with the development of these models is that they have not been informed by micro-scale experiments to elucidate the mechanism and therefore lack the necessary physical basis and validation. Techniques for monitoring early signs of bearing damage were established by Fuentes et al. [25], using AE hit (data from a single burst of AE) parameter statistics such as maximum amplitude, rise time, and duration.

Research processing AE in the frequency domain was initially done using wavelet transforms [26]. More recently, Reddyhoff et al. used short time Fourier transforms (STFT) to show that certain AE frequencies correlated with friction coefficient [27]. However, neither the frequencies nor the constants of proportionality linking AE and friction were known prior to testing. Then, Strablegg et al. [28] used both STFT and Superlet transforms to process AE and linked spectral aspects of these results to tribological parameters. Baccar and Söffker [29] used both STFT and continuous wavelet transform (CWT) to quantify AE energy and identified different phases in wear progression from the frequency spectrum produced. Hase et al. [30] distinguished between abrasive and adhesive wear mechanisms from different regions in their frequency spectrum. Fuentes et al. [31] also showed clear differences in spectral analysis of its AE bursts from plastic deformation. These works indicate that the frequency spectrum is rich in information relating to in-contact friction and wear mechanisms.

Overall, these studies demonstrate a clear need and interest in developing acoustic emission techniques for machine condition monitoring, and the potential for AE to accomplish this. However, there are few studies on how AE responds to varying contact conditions such as sliding speed and normal load. While some of the empirical [16, 17] and theoretical models [22] include parameters relating to speed and normal load, there is little work done to verify these. Most experiments recording friction coefficient so far have been conducted at a fixed load and speed, and although the models produced may seem reliable, they are applied to a very narrow and idealised set of contact conditions. This shortcoming is significant since friction is a system property rather than a material property.

The current paper applies machine learning (ML) to AE data from a steel-on-steel oscillating contact to predict friction under a range of conditions. There have been some examples of ML being applied to acoustic emission data. These include (1) classifying of the type of wear mechanism [32], (2) maximum energy barrier at the onset of sliding of a single layer 2D [33], (3) classifying of average friction over a whole test [34], (4) classification of frictional power over 20 ranges/classes [35]. Our current study is novel in that it is the friction coefficient that is predicted. Furthermore, it is predicted continuously in time over the duration of the test, and continuously over the full coefficient of friction range. This high precision prediction has, to our best knowledge, not been attempted before. Also, five pre-processing methods to reduce AE data are tested: down sampling, trimming, AE root mean square (RMS), short time Fourier transforms, and short time histograms. These are input into the ML models to relate coefficient of friction to AE. This is done for tests under a range of conditions with varying normal load, stroke speed, and stroke length. The trained ML models are then used to predict friction based on new, unseen AE data from tests at varying conditions. These predictions are both accurate and robust, under all test conditions.

2 Experimental setup

2.1 Testing apparatus

The experiments involved a ball-on-disc rubbing contact operated by a high frequency reciprocating rig (HFRR) from PCS Instruments (Fig. 1). An upper ball specimen is attached to a reciprocating arm, while the lower disc specimen is fixed to a stationary base. The ball is 6 mm in diameter and made of AISI E-52100 Steel with a hardness of 58–66 HRC and polished to a surface roughness of less than 0.05 μm. The disc is 10 mm in diameter and machined from an annealed AISI E-52100 steel rod with a hardness of 190–210 HV30 and polished to a surface roughness of 0.02 μm. A constant normal load to press the ball and disc together was applied by hanging dead-weights off the upper specimen holder. The stroke length and frequency of the reciprocating motion were varied by changing motor parameters. The ball and disc samples and holders were ultrasonically cleaned with toluene and then 2-propanol, for 10 minutes each before each test. The coefficient of friction was measured directly using a force transducer attached to the lower disc holder. Since the holder is constrained by a flexible support of known stiffness, the friction force is transmitted to the transducer and is calibrated accordingly. The sampling frequency of 1 Hz so that each friction data point is an average over many cycles. Repeat tests were run under each different set of conditions.

An acoustic emission sensor (micro 200 HF, from Physical Acoustics, Mistras group) is bonded to the front of the base that holds the lower specimen holder using cyanoacrylate, at a position 19 mm away from the center of the disc specimen as shown in Fig. 1(a). The sensor is connected to a Mistras 2/4/6 Preamplifier set to 40 dB, allowing a range of ± 10 V to be measured, as well as a bandwidth range of 10 kHz–2 MHz. The signal generated is digitally sampled at a 2 MHz rate by the Mistras, PCI-2 Analogue to Digital (A/D) card. This data was finally acquired and saved using AEWin software before processing in Matlab.

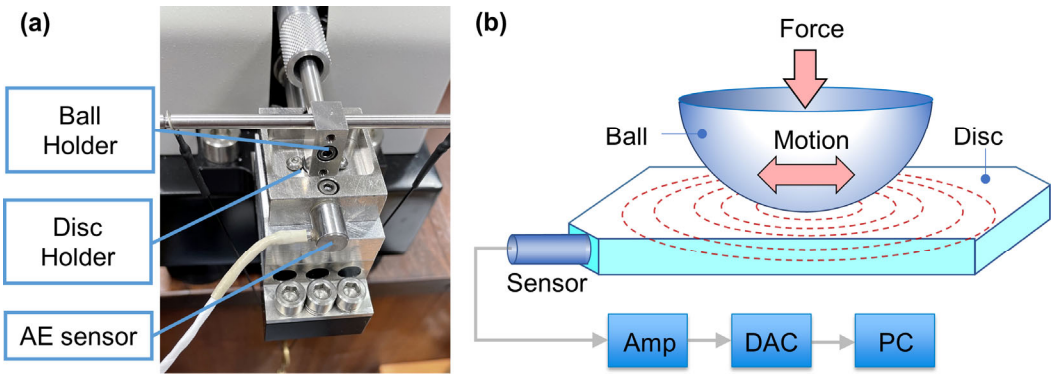

Fig. 1 (a) Photo of HFRR test rig and (b) schematic of experimental set-up involving ball on disc sliding contact.

2.2 Test conditions

All HFRR rubbing tests were conducted under dry, unlubricated conditions, at an ambient temperature of 20 °C for a duration of 10 minutes. Initial baseline tests were run at 4 N normal load, 50 Hz reciprocating frequency and 1 mm stoke length. Then, these test conditions were systematically varied, with loads from 4 to 6 N, frequencies from 25 to 125 Hz, and stroke lengths from 1 to 2 mm. The full set of test conditions is shown in Fig. 2. Tests at each of these conditions were repeated three times and named as shown in Table 1. The Hertz contact radius for these loads varies between 42 and 48 μm, which compared to the mm stroke lengths suggests gross sliding occurs rather than fretting occurs during these tests.

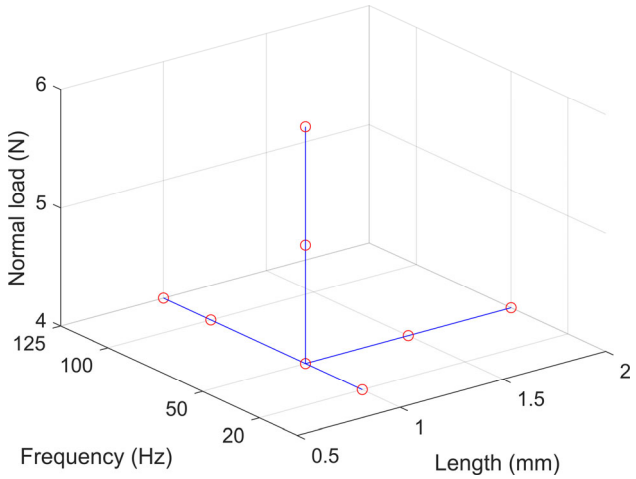

Fig. 2 3-D plot showing how the HFRR test conditions were systematically varied against each other. Tests and their repeats were done for each red point.

Table 1 List of all test conditions studied, and their repeats.

Test name (Number. Repeat)	Applied load (N)	Reciprocating frequency (Hz)	Stroke length (mm)
1.1 – 1.3	4	50	1.5
2.1 – 2.3	4	50	2
3.1 – 3.3	4	25	1
4.1 – 4.3	4	100	1
5.1 – 5.3	4	125	1
6.1 – 6.3	4	50	1
7.1 – 7.3	5	50	1
8.1 – 8.3	6	50	1

3 Initial AE data analysis

An example of unprocessed AE and friction data from a test is shown in Figs. 3(a) and 3(b). The friction signal from the HFRR force transducer varies over time. Initially, there is a static friction peak due to the prolonged pressing of the specimens prior to sliding. Subsequently, the friction varies due to the evolution of wear in the contact, which causes the real area of contact and the material properties and topography of the interface to changeover time (e.g., due to plastic deformation and oxidation as reported in Ref. [27]). The AE and Friction traces look very different here. However, AE data is abundant in tribological information as suggested by previous research [6, 36], and demonstrated by the processing techniques presented below. Figures 3(c)–3(f) show successive zoomed in sections of the AE signal. In Fig. 3(c) it becomes clear that most of the points are concentrated close to zero volts. Further in Fig. 3(d), distinct AE bursts become visible. Zooming further in to Figs. 3(e) and 3(f), individual AE waves become clear. At these scales, it becomes apparent that AE waves are composed of many frequencies. Interestingly, the friction signal increases to close to maximum amplitude at the onset of sliding, whereas AE signal initially shows very low amplitude before a rapid increase in activity occurs after ~100 s of rubbing. This may be attributed to a change in wear mechanism, which AE is more sensitive to. SEM imaging of worn surfaces from similar tests [27] suggested this may be due to oxide layers forming/cracking to produce rapid/high amplitude AE events which does not greatly affect the friction coefficient. This is supported later by Fig. 7(d), where it is the low voltage AE events that correlate best with friction coefficient.

The high AE acquisition rate (2 MHz), which is necessary to capture tribological events, produces large data files rapidly (18 GB per 10-min test). To be able to form correlations using machine learning regression techniques using practical computing capacities and time constraints, this data must be reduced in size. Five ways of doing this are presented and assessed in the following section.

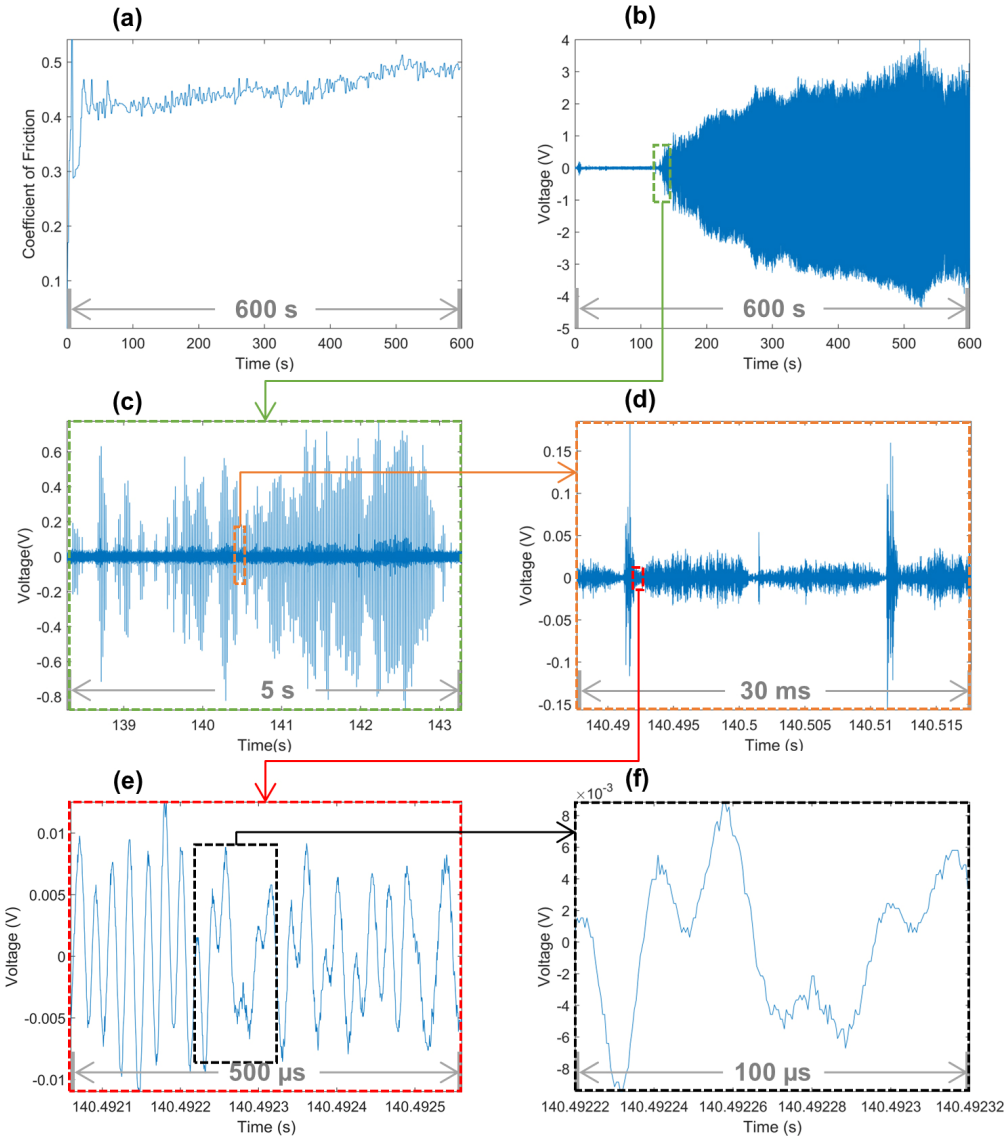

Fig. 3 Initial results for a 1.5 mm, 50 Hz, 4 N test. (a) Friction data. (b)–(f) Zoom in of AE data.

4 AE data processing

The data reduction methods involve dividing the full AE signal into short time windows and then reducing the data in each of these windows. For an $n = 600$ s long test, time windows of 1 second were chosen which gives one AE segment per friction coefficient measurement (since friction was measured at 1 Hz). Each of these 1 second windows of AE signal originally contained 2×10^6 data points, and it was required to reduce this by a factor of $i = 500$, leaving approximately $j = 4{,}000$ points per second. Data in this reduced form could be used, along with the corresponding coefficient of friction signal, to train and then test the machine learning models. Considering that data from many tests must be concatenated to form the training array for machine learning, this factor of reduction makes the data small enough that it can be processed effectively by the machine learning algorithms (No. tests × No. windows in a test × (No. AE points in a window + No. friction points in a window) = 16 × 600 × (4,000 + 1) = 3.84096×10^7 total points used for training). The data reduction process is summarised in Fig. 4.

4.1 Time based methods

Three different time domain methods were used to

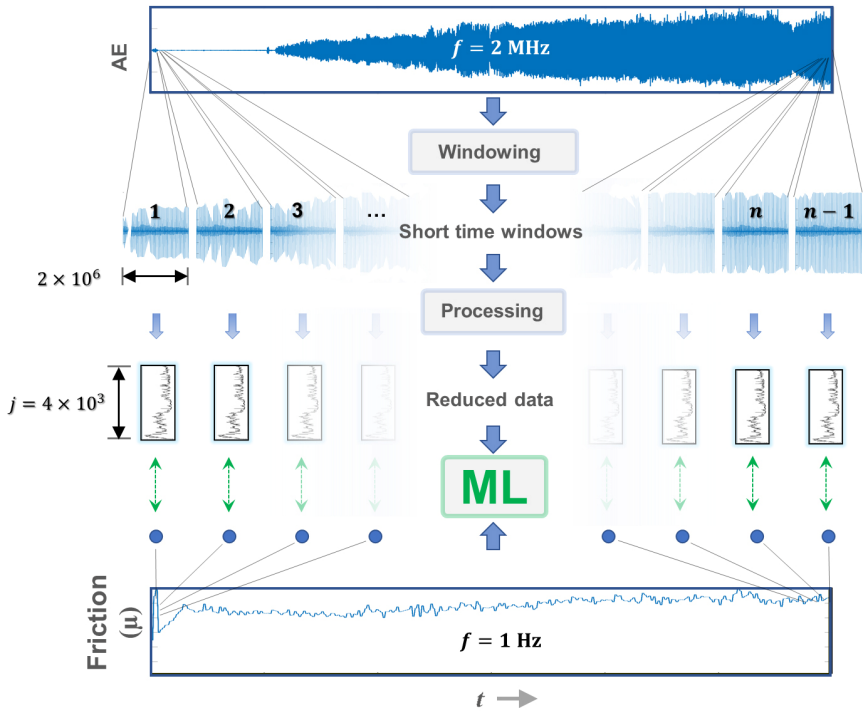

Fig. 4 Data processing scheme.

reduce the AE data:
(1) Down sampling;
(2) Trimming;
(3) Root mean square (RMS) averaging.

When down sampling is used, one out of every i AE data points are taken while the rest are discarded. This effectively lowers the sampling frequency by a factor of i. The resulting 1 s duration windows of AE data can then be rearranged into a $j \times n$ array as shown in Figs. 5(a) and 5(b).

When trimming is used, the first j points out of every second of AE data are taken while the rest are discarded, as shown in Figs. 5(c) and 5(d). This maintains the original sampling frequency, but the signal is no longer continuous.

When RMS averaging is used, every i points in the AE signal are used to calculate the root mean squared average, reducing them to one point. This effectively reduces the sampling frequency as did down sampling, but now the averaged point is informed by many points around it. This is shown in Figs. 5(e) and 5(f).

4.2 Short-time Fourier transform

The short-time Fourier transform (STFT) is a time-frequency domain method. The AE signal is divided into short time windows, and the fast Fourier transform (FFT) is applied to each of them. The resulting FFTs are then stacked together to create the spectrogram array showing how the amplitudes at each frequency step change with time. This approach is described in Figs. 6(a) and 6(b).

The window size is carefully chosen as this determines the resolution in the time and frequency domains (a larger window produces a better frequency resolution, while a smaller window produces a better time resolution and requires less computation time). A window containing 7,575 points was chosen, giving a frequency step of 244 Hz and a time step of 0.0038 seconds. This gives a reasonable frequency step, while maintaining manageable processing times. This was then averaged down to one point per second, producing a final spectrogram array of (4,097 × 600).

The intensity variation in each horizontal line of the resulting STFT spectrogram array gives the temporal variation in AE amplitude at that frequency. As exemplified in Fig. 6(c), the amplitude of certain AE frequencies vary in a similar way to the friction coefficient. To characterise this, Fig. 6(d) plots the correlation coefficient between the amplitude of each

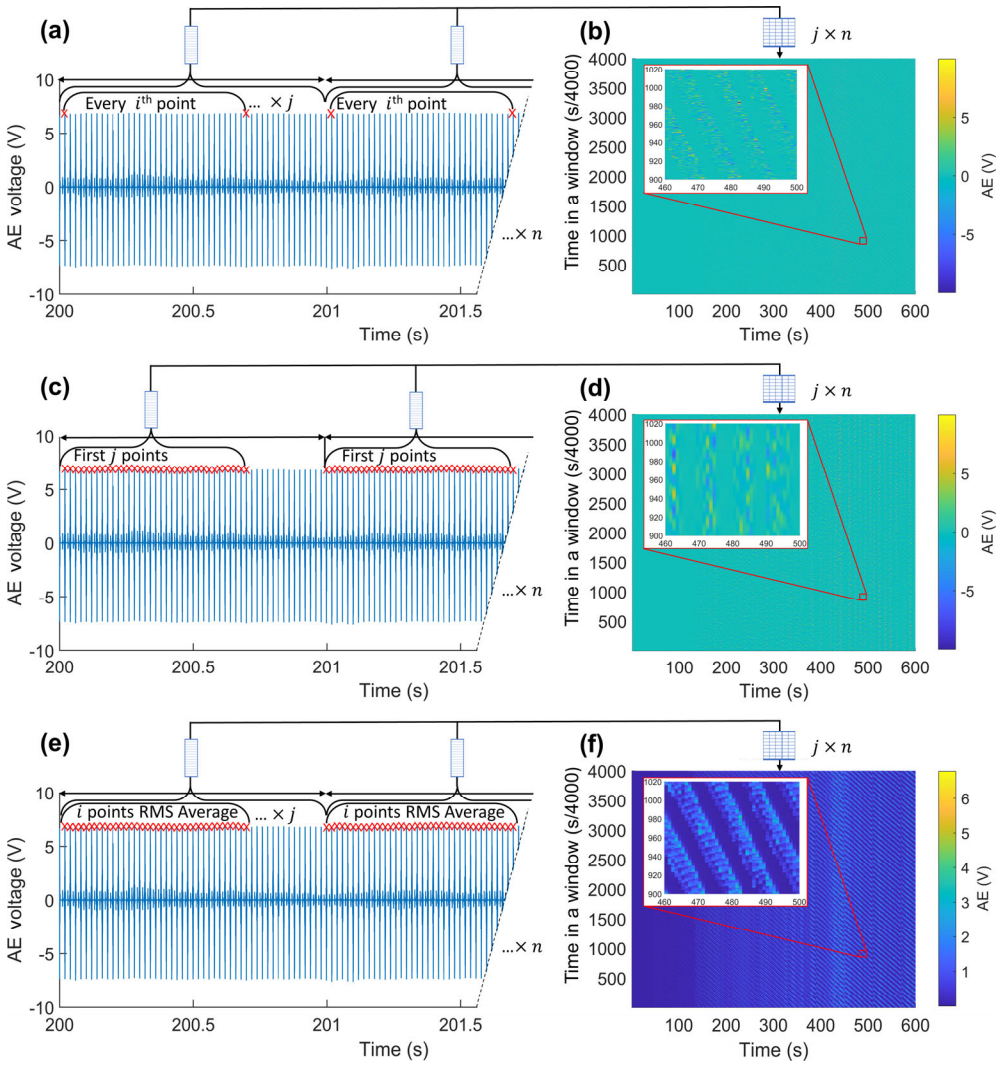

Fig. 5 (a) Schematic representation of down sampling method and (b) resulting array. Many of these points are close to 0 V, but zooming into the plot reveals some brighter points where the AE bursts have been captured. (c) Schematic representation of method to trim AE data by taking the first j points of individual time windows, and (d) the resulting array. (e) Schematic representation of RMS averaging and (f) the resulting array.

AE frequency and the friction coefficient. Figure 6(d) shows high correlations are found across most of the frequency spectrum, which suggests this form of the AE data presents friction behaviour meaningfully and may indicate its suitability as an input for the machine learning models.

4.3 Short time histogram (STHG)

Supposing that each burst in the AE data corresponds to a single AE event, the magnitude of a burst may be related to the mechanisms which produced it. This implies that bursts of similar magnitude may be produced from similar mechanisms. Typically, AE signals are processed by counting the times the AE signal exceeds some threshold (i.e., counts are often reported [16, 37, 38]). However, here the approach is extended by dividing the AE voltage range into subranges (i.e., histogram bins) and counting the number of times AE data points fall into each bin. In this way, changing AE mechanisms can be monitored in time, by effectively counting the number of bursts at a given magnitude. To explore this, histogram bins (voltage subranges) were set up to cover the whole voltage range of the AE signal (±10 V). Then, every AE data point within a time window was sorted into a bin based on its voltage and counted. In Figs. 7(a)

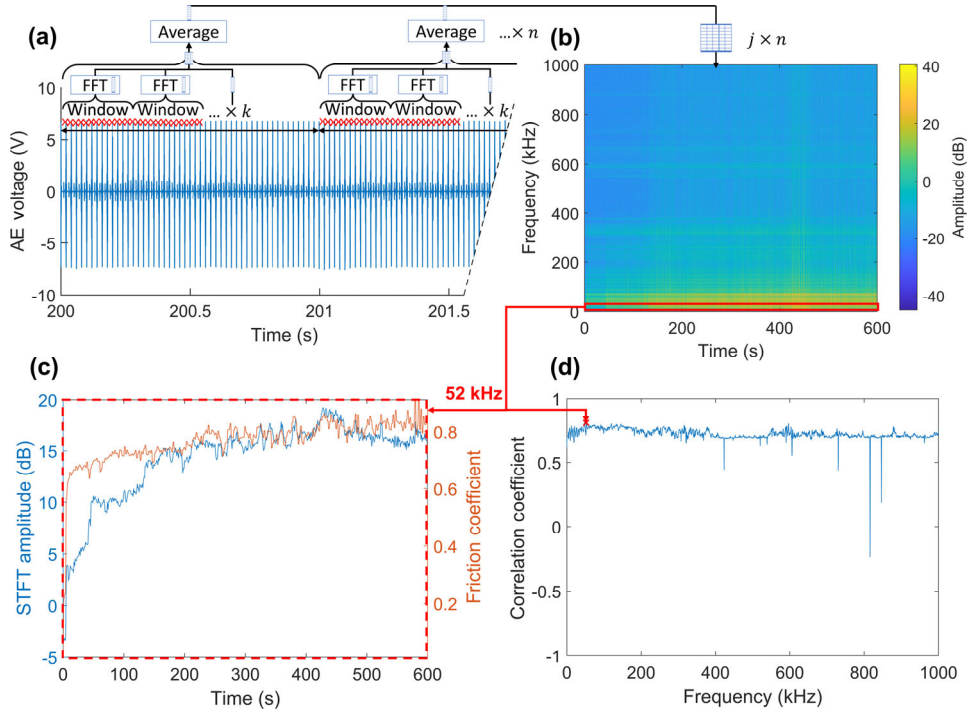

Fig. 6 Short-time Fourier transform. (a) Schematic representation STFT method, which involves: applying an FFT to a short time window of AE data, and repeating this for the rest of the signal before concatenating resulting data to a single array. (b) Stacked FFTs are plotted in a spectrogram, showing how the frequency response changes with time. (c) Variation in friction coefficient and FFT amplitude of a frequency of 52 kHz with time. (d) The correlation coefficient between the amplitude of each AE frequency and the friction coefficient.

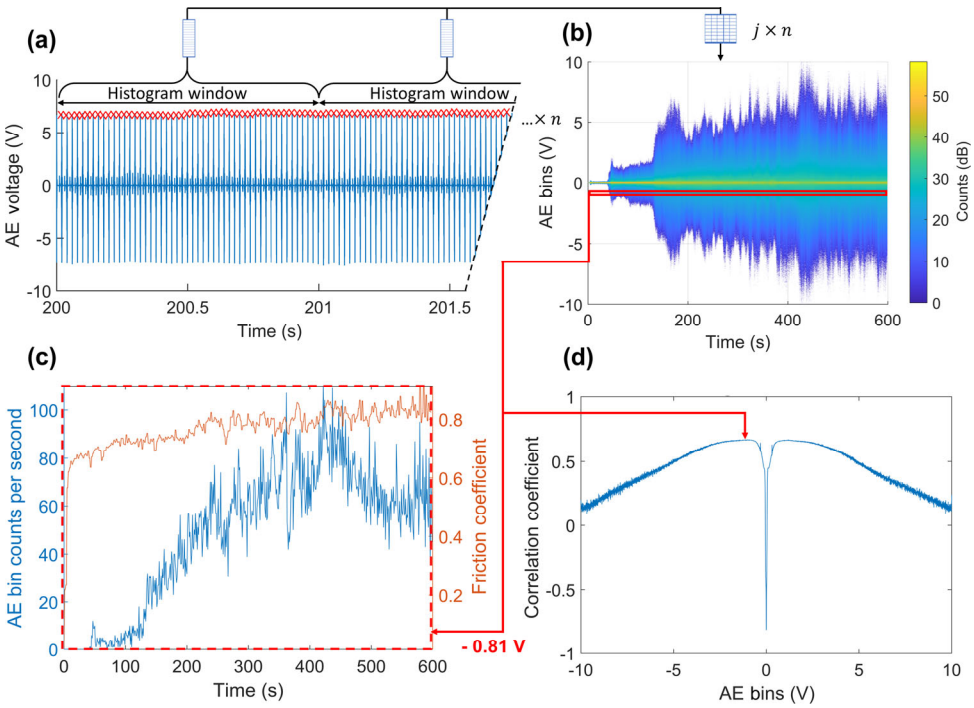

Fig. 7 Short-time histogram. (a) Schematic representation STHG method, which involves making a histogram from a short time window of AE data and repeating this is for the rest of the signal, before concatenating resulting data to a single array. (b) Stacked histograms are plotted, showing the voltage bin count distribution changes with time. (c) Variation in friction coefficient and AE bin count rate with time for a bin with a discrete AE voltage level of –0.81 V. (d) The correlation coefficient between the counts in each voltage range/bin and the friction coefficient.

and 7(b) these short time histograms (STHG) have been then stacked together into an array analogous to the STFT spectrogram array. As with the other reduction methods, the window length is 1 second in duration so that one histogram is obtained for every friction data point recorded at 1 Hz acquisition rate.

The AE signal has a ±10 V range. However, as can be seen from Fig. 7(b), most of the points are concentrated around 0 V. Therefore, to reduce the data by a factor of $i = 500$ while maintaining as much AE information as possible, a histogram applied to a range of ± 0.625 V was used (datapoints with a magnitude greater than 0.625 were ignored). Each histogram bin width was set to be equal to the voltage resolution of the digitised AE signal, (so each discrete AE voltage level had its own bin). For the 16 bit digitiser used by the AE DAQ, this produced $2^{16} \times 0.625/10 + 1 =$ 4,097 voltage bins for the ±0.625 V. From these results, the temporal variation of AE counts with a particular voltage range/bin can be obtained by taking a horizontal line in the STHG. This signal was then correlated with the friction coefficient for each bin.

As exemplified in Fig. 7(c), the number or AE counts within certain voltage ranges vary with time in a similar way to the friction coefficient. To characterise this, Fig. 7(d) plots the correlation coefficient between the number of counts at each AE voltage range and the friction coefficient. Here, the correlation with friction increases as the 0 V bin is approached from both positive and negative directions. At voltage bins very close to 0 V, there is a strong anti-correlation (this may be because a data point falling within a zero-voltage bin indicates that higher voltage levels bins are empty and hence no friction events/energy dissipation mechanisms are occurring at that moment). This supports the approach of reducing the histogram range to ±0.625 V as it focusses on bins with a strong friction correlation. It also suggests that AE data in this form represents friction behaviour meaningfully and is hence a suitable input for the machine learning models.

5 Regression machine learning

5.1 Algorithms

The correlations presented in Figs. 6(d) and 7(d) indicate that the AE signal contains rich tribological information relating to the friction coefficient. However, due to the complexity of the processes occurring, the exact relationship between these two signals is unclear (i.e., the coefficient of proportionality is unknown) and therefore it has proved difficult to predict friction based on AE data. Using machine learning regression techniques to establish this link offers a way around this obstacle.

To form predictions of friction coefficient from AE data, multiple variable linear regression methods were chosen, meaning they can take many predictor points from the AE data array, and relate them to one friction point, the response variable [39]. This means, for example, that all the AE frequency components or voltage bin counts at a particular time are used to predict one point at the corresponding time in the friction signal. In this way all the data in the reduced $j \times n$ arrays are used for the machine learning. Two different algorithms, a Gaussian process regression model (GPR) and a support vector machine model (SVM), were tested. Other ML methods such as linear regression and decision trees were assessed, but these were less accurate than GPR and SVM and therefore, for reasons of brevity, their predictions have not been reported here.

The GPR models are nonparametric kernel-based probabilistic models [40, 41]. These models predict points using all input data but give more weight to training points that are near the points to be predicted. The kernel function defines how the distance from the training points to the points being predicted influences the weight those training points have on predictions. Here an exponential kernel function was chosen, creating a Gaussian distribution describing the influence of training points for predicting a point, where close data points strongly influence the prediction and as training points get further away their influence declines. These kernel functions are setup for every point in the training array so that when predicting a query point a combination of all the influence of points from all kernels is used to calculate a prediction.

The second algorithm tested was SVM. Although SVM is widely used in classification models, it can be adapted to regression models as well [42, 43]. This method works by defining a hyperplane through the

data, based on a previously chosen kernel function. The hyperplane parameters are then found based on minimising the distance from that hyperplane needed to envelope all the data.

5.2 Training and validation procedures

The two ML algorithms were applied to the five different AE data processing methods detailed in Section 4. By inputting the five different reduced AE data arrays into each of the two machine learning algorithms, a total of ten different data processing/algorithm combinations can be formed for a single set of friction tests. Once the model is trained, new AE data can be fed in, and it will output its prediction of friction coefficient. Figure 8 summarises this procedure used to train and evaluate the machine learning algorithms in predicting friction based on AE data.

As the machine learning models allow reduced AE data from many tests to be used for training, different combinations of test data inputs were explored. First, a set of machine learning models were formed for each test condition (i.e., for a specific load, speed, and stroke length). Two test repeats at each condition were collected and concatenated together to form the machine learning training input. The third test, performed under the same set of conditions, was reserved for validating the model performance afterwards. For instance, each ML algorithm was trained using friction and AE data from repeat tests 1.1 and 1.2 (4 N load, 50 Hz reciprocating frequency, and 1.5 mm stroke length), and the resulting model used to predict friction based on AE data from repeat test 1.3, obtained under the same conditions. The accuracy of this prediction was then assessed by comparing it with the corresponding directly measured friction from test 1.3. This process (i.e., using the same test conditions for both training and validation) was applied separately to each row of Table 1 to assess how accurately the machine learning models can predict friction based on AE data under each set of conditions. This produced 8 different condition specific models (CSM) for each condition.

Next, a larger input test array was considered, comprising data from all test conditions 1 to 8 listed in Table 1. This training array was formed from concatenating data from test repeats 1 and 2 at every condition, while the validation arrays come from the third test repeat at every condition. Hence, this single

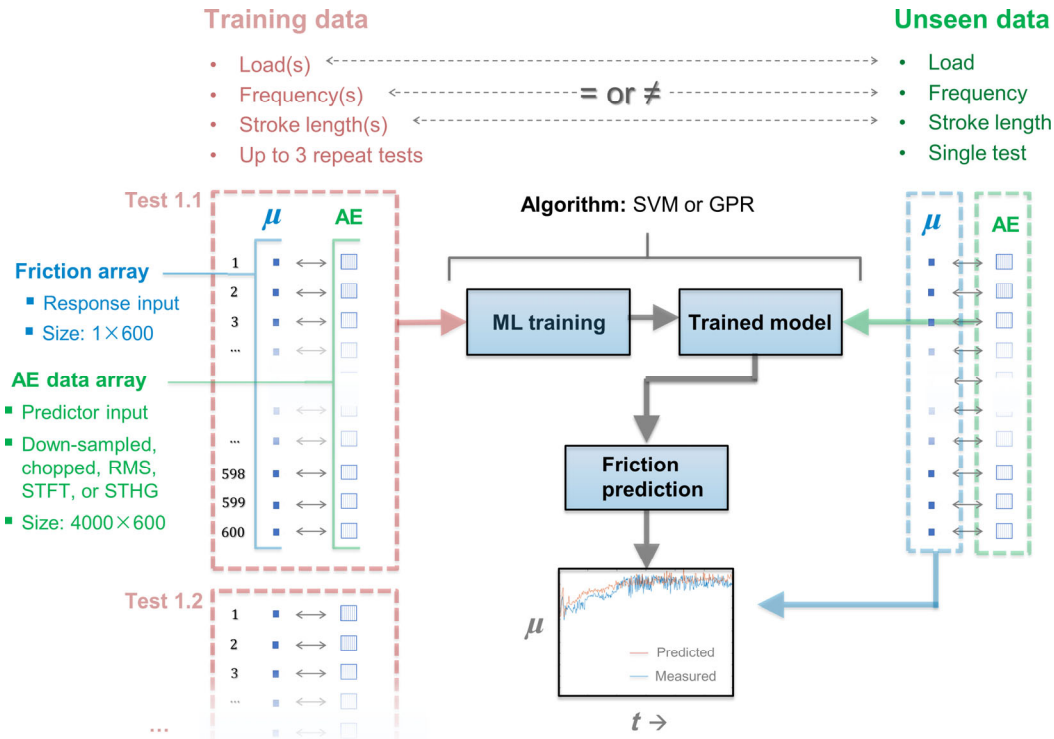

Fig. 8 Summary of procedure to train and evaluate the machine learning algorithms in predicting friction based on AE data.

model is validated 8 times by each of the different test conditions. This approach uses more data to train the machine learning (here 2×8 = 16 tests were used in a single training array, as opposed to 2×1 = 2 tests used for each training array described in the section above), so that the resulting single condition generic model (CGM) can then be universally applied to any of the unseen AE test data, irrespective of the test conditions. The accuracy of the resulting friction predictions was assessed by comparing with the corresponding measured friction under each condition.

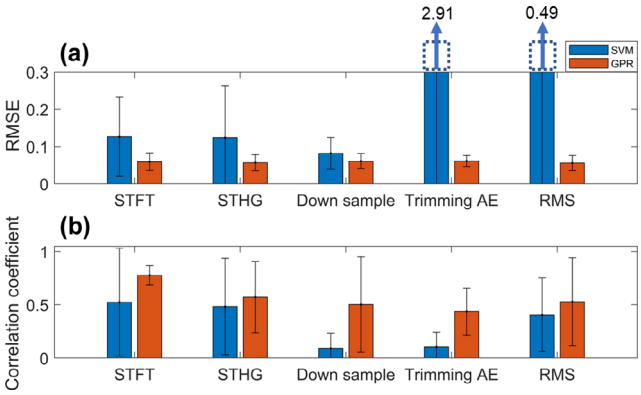

Fig. 9 Mean model evaluation parameters for tests at the same conditions. (a) The average RMSE error. (b) The average Pearson correlation coefficient.

6 Results

To evaluate each machine learning model, the Pearson correlation coefficient (r) and the root mean square error (RMSE) were calculated for each model prediction. The r measures the linear correlation between the measured and predicted friction, and the RMSE measures how accurate the absolute values of the predictions are. A model with a strong performance will have both a high r value and low RMSE. These evaluation parameters were averaged across the predictions from each model, and the highest and lowest RMSE and r values from each model were noted.

6.1 Condition specific model (CSM)

First the performance of the CSM models was assessed, where both training and validating data were obtained under the same conditions. Test data underwent the processing methods described in Section 4 and were then concatenated to form the training arrays. The training arrays were then processed by both GPR and SVM algorithms. This procedure was repeated for each set of test conditions, from 1 to 8 in Table 1, resulting in a total of 80 models (No. processing methods × No. algorithms × No. test conditions = 5×2×8=80). The resulting models were then evaluated. The r and RMSE values were calculated for each model and averaged across the test conditions to compare the processing methods and ML algorithms (Fig. 9).

The GPR algorithm gives a stronger correlation and smaller RMSE error across all the models, with the GPR applied to the AE RMS array giving the smallest average RMSE of 0.056. Although the AE RMS GPR model had the smallest average RMSE of 0.056, the correlation r spread across tests made it less reliable (note standard deviation error bars). Overall, considering both RMSE and r, the GPR combined with STFT array appears to be the most accurate, with the STFT GPR model demonstrating an average RMSE value of 0.0593 and an average correlation coefficient r of 0.777. Both the measured friction and the friction predicted by this model, using tests repeated at the same condition for the STFT GPR model are shown below in Fig. 10. Full figures of the predictions from every CSM model can be found in Appendix Fig. A1.

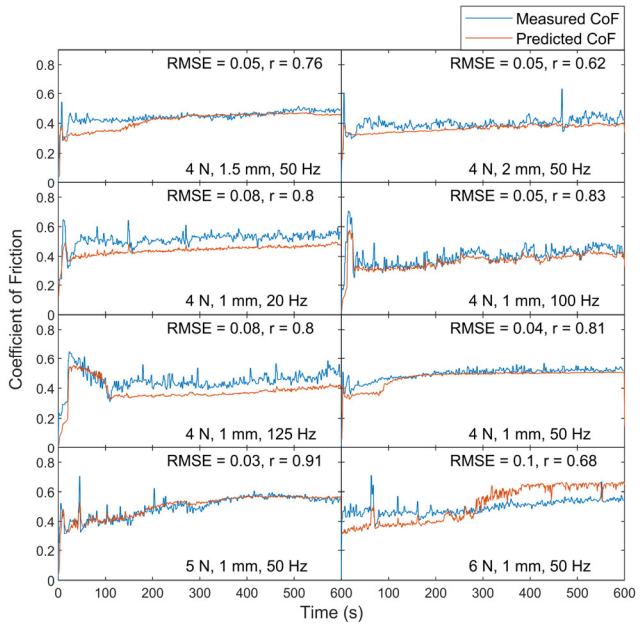

Fig. 10 Measured friction and model predictions from the GPR STFT models—training and validation test data obtained under the same conditions.

The close agreement between the AE-predicted friction and the directly measured friction demonstrates the potential of the proposed approach, with r reaching values up to 0.91 and RMSE getting as low as 0.03. However, the trained models used here are very specific to the particular set of test conditions used for training, and therefore would have limited use in practical applications where test conditions vary and may not be known.

6.2 Condition generic model (CGM)

Pearson correlation coefficient r and RMSE were also used to assess the Condition Generic Models, which were trained with a single set of data concatenated from test repeats 1 and 2 at all conditions, and subsequently applied to all repeat 3 tests. The results were then averaged across all the test conditions to compare the processing methods and ML algorithms and summarised in Fig. 11.

Overall, the CGM models are stronger than the CSM models, as the RMSE error is generally lower. This could be due to the larger training arrays used for these models. Complete graphs of the predictions from every CGM model can be found in Appendix Fig. A2. The GPR algorithm applied to the Histogram array was identified here as the strongest model, with the lowest average RMSE of 0.0529, an average correlation coefficient of 0.56. Although the STFT GPR model showed a higher correlation coefficient, the RMSE was prioritised as an evaluating parameter, as this determines the model accuracy. Therefore, STHG GPR model was deemed the strongest model. The

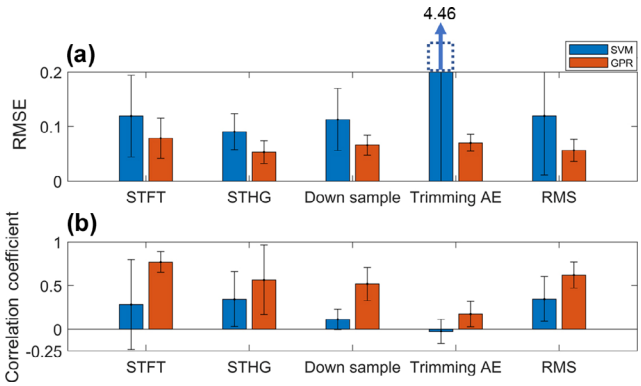

Fig. 11 Mean model evaluation parameters for tests trained from all conditions. (a) The average RMSE error. (b) The average Pearson correlation coefficient.

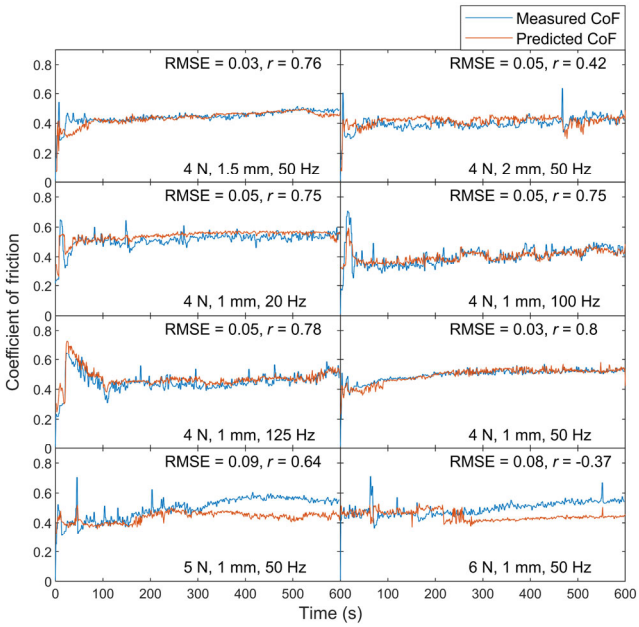

Fig. 12 Measured friction and model predictions from the GPR STHG model trained from different test conditions.

friction predicted using this model is plotted alongside the directly measured friction in Fig. 12. The agreement between the AE-predicted and the measured friction is still strong, with correlations up to 0.8 and RMSE errors down to 0.03. This single model can cope well with the changes in load, stroke length, and oscillating frequency, demonstrating much more potential for use in practical applications. The model predictions for 5 and 6 N seem to develop an offset error after about 300 seconds, but still maintain a correlation. As these tests are at higher loads, this could indicate that the underlying wear mechanisms are changing around this time and consequently the fundamental relationship between AE data and friction is changing. It is suspected that this is due to the formation of oxide layers on the sliding surfaces, as noted by Geng et al. [27], who observed increasing amounts of oxide debris forming on the surface as test load was increased. Furthermore, such oxide layers were found to cause increased acoustic noise without affecting friction greatly. It is also interesting that for these tests, especially those at high HFRR oscillating frequencies, the AE can predict not only absolute magnitude and overall trends, but also transient variations in the friction signal. This precision currently cannot be achieved by applying classification methods to discretised friction data.

6.3 Discussion

These results demonstrate the effectiveness of applying machine learning to acoustic emission data to predict friction coefficient and the importance of selecting an appropriate pre-processing technique. The CGM models presented have much stronger agreements with the measured friction than the CSM models do. Using the larger training data array greatly increases the model performance, even though this data comes from a mixture of different test conditions. However, using more data also requires more time to train the machine learning models. This raises the question of what the ideal amount of data is, for an optimal compromise between model performance and training time. Further studies should be done, for instance by systematically removing data to improve training times while minimally affecting prediction accuracy. This could be approached in two ways, either using fewer tests for training, or increasing the reduction factor i of the data processing methods. The former could involve being more selective with the tests used, e.g., removing some of the repeated tests. The latter would require reducing each window to fewer points. Figures 6 and 7 show that some frequencies and bins show stronger correlations with friction than others, and suggesting they are more important for making predictions. Data could be further reduced by being more selective with which bins/frequencies are chosen to input into the machine learning. Larger frequency steps or wider histogram bins could also be considered when processing the STFT and STHG.

Machine learning training time is also dependent on the algorithms used. Generally, the GPR algorithm requires more time to train, as it must calculate a gaussian distribution for each point, whereas the SVM focuses more on the extreme data points to calculate its hyperplane boundary. On the one hand, this makes SVM more suitable for larger data sets, but on the other the GPR can produce stronger predictions as demonstrated in Figs. 11 and 9. More work is required to characterise how these algorithms respond with different base kernel functions and explore AE data processing with other ML algorithms.

During these tests, wear states will likely vary between abrasion, adhesion, and oxidative as suggested in Ref. [27]. As these interlinked processes occur, the initially mirror-polished contacting surfaces evolve into ~1 mm wear scars with intricate/disordered micro-scale morphology and inhomogeneities. This all must affect the friction coefficient. However, such information is not explicitly required since the machine learning models are trained to predict friction from the acoustic emission as wear states vary. It is not apparent how the ML models do this, but they could for example use parts of the acoustic signal to ascertain the wear state and use this to adjust the relationship between emission and friction appropriately. Another intricacy that the machine learning handles is that the recorded AE signal will include not only the stress waves generated in the sliding contact, but also the effects of frequency response of the sensor/amplifier and the modes of vibration of the test set up which are excited during the test.

The effectiveness of machine learning algorithms in linking friction and acoustic emission, suggests that these phenomena must be closely related. However, few studies have probed the micro-scale tribological mechanisms that produce high frequency sound in sliding contacts, and so there is no robust theoretical relationship between friction and acoustic emission. Therefore, possible reasons for the correlations are speculated upon as follows. Plastic deformation is the dominant means of energy dissipation in our unlubricated sliding contact, due to high interfacial pressures on the ductile steel specimens. This is clear from images of plastic wear from our experiments [27]. Plastic deformation in tensile tests is known to generate acoustic emission caused by dislocation glide [44, 45], mechanical twinning [46], and interaction of dislocations with solute atoms [47, 48] Moreover, due to dislocation avalanching [49], AE has been shown in these plastic tests to be intermittent in nature and thus commensurate with the burst like behaviour observed in our measurements Fig. 3. An insight into the relationship/proportionality between the extent of plastic deformation (number and/or intensity of dislocation avalanches) and the magnitude of the friction coefficient maybe gained by considering adhesion behaviour. According to the Bowden and Tabor model for solid–solid adhesion [50], contacting asperity peaks deform plastically until the real contact area, A_c, is just large enough to support the normal

load, L, ($L = A_c H$, where H is the hardness). Neglecting ploughing effects, the force, F, to shear the interface is the product of the shear strength of these conjunctions and their total area ($F = A_c \tau_f$). The resulting coefficient of friction due to adhesion ($\mu = F/W = \tau_f/H$) is independent of applied load as required but under-predicts friction. Junction growth must therefore occur, whereby normal load and shear force couple to produce additional plastic deformation to increase the contact area and thus friction. Taken together, this may suggest that the relationship between friction and AE that the ML algorithms have found result from both of these phenomena being dependent upon the real contact. However, evidently from Fig. 7(d) there are many AE points, some with substantial magnitude, which do not correlate well with friction. This suggests that AE also arises from other mechanisms at the contact which do not contribute to friction. These could originate from the formation of wear particles, or subsurface crack formation. It may therefore be that the ML algorithms are filtering out aspects of the AE signal which relate to frictionally non-contributing mechanisms. The sensitivity of AE to plastic deformation also highlights the former's suitability for wear and failure monitoring. The above is highly speculative and warrants further research possibly involving in situ measurements and atomic-scale modelling.

Overall, these results show that AE acquisition and processing is a promising way to predict friction in sliding contacts and may be developed to monitor lubrication and frictional dissipation/efficiency. However, some differences between lab settings and industrial applications should be noted here. Within the lab the AE sensor was placed close to the contact to ensure the data obtained comes from the contact between specimens of known material and roughness. In practical applications, physical space limitations within an assembly or working conditions (temperature limits) may require sensors to be placed further away. AE from the sliding contact will attenuate before reaching the sensor, and the sensor will be more susceptible to recording noise from other unwanted sources. Furthermore, the component material and roughness may be poorly defined in practice. Therefore, future work is necessary to develop robust ML-AE techniques trained on a wider set of test data covering the relevant conditions. This may be combined with optimized sensor location and possibly using multiple sensors placed around the contact to distinguish AE from the contact from other sources.

Furthermore, once the rich acoustic signal can be better interpreted and understood, AE measurements may a useful addition to lab based tribometer measurement systems in order to provide real-time information on friction and wear mechanisms. This would supplement currently prevalent optical, electrical and active acoustic measurement methods. Compared to these, AE may also be lower cost and lower equipment complexity since the energy is generated in the contact itself and does not require an additional power source.

7 Conclusions

We trained machine learning algorithms (SVM and GPR) to correlate acoustic emission with continually varying friction in a steel-steel rubbing contact. This required the dense AE data to first be reduced in size. A range of processing techniques were assessed for this, and short time Fourier transform and histograms seemed to condense the data in the most meaningful and effective way. The trained models were then tested with fresh, unseen AE data and the resulting predicted friction compared with transducer measurements of friction. The excellent agreement between the measured and predicted friction (characterised by low RMSE error and a strong correlation coefficient) was shown when the GPR model was used on the histogram data. Moreover, predictions remained accurate (able to capture friction variations occurring at different timescales) despite changes in test conditions such as normal load, reciprocating frequency, and stroke length. Predictions became less accurate at higher loads, most likely due to noisy oxidative wear and would require more training at these conditions. These results suggest that:

1) AE monitoring combined with machine learning, AE-ML, may be an effective means of monitoring rubbing contacts to increase efficiency and predict failure. In practice, this requires models to be trained on real machines with varied sources of background noise and poorly defined conditions.

2) There must be microscale mechanisms linking friction coefficient and noise generation, and we hypothesize these may involve plastic deformation around the real area of contact which causes both sliding resistance (friction) and dislocation bursts (AE).
3) Machine learning may be an effective tool in other tribological applications where mechanisms are poorly defined.

Appendix

The plots for predicted and measured friction coefficient from all the CSM models are shown in Fig. A1.

The plots for predicted and measured friction coefficient from all the CGM models are shown in Fig. A2.

Acknowledgements

This study was supported by a UK Engineering and Physical Sciences Research Council Ph.D. studentship.

Declaration of competing interest

The authors have no competing interests to declare that are relevant to the content of this article.

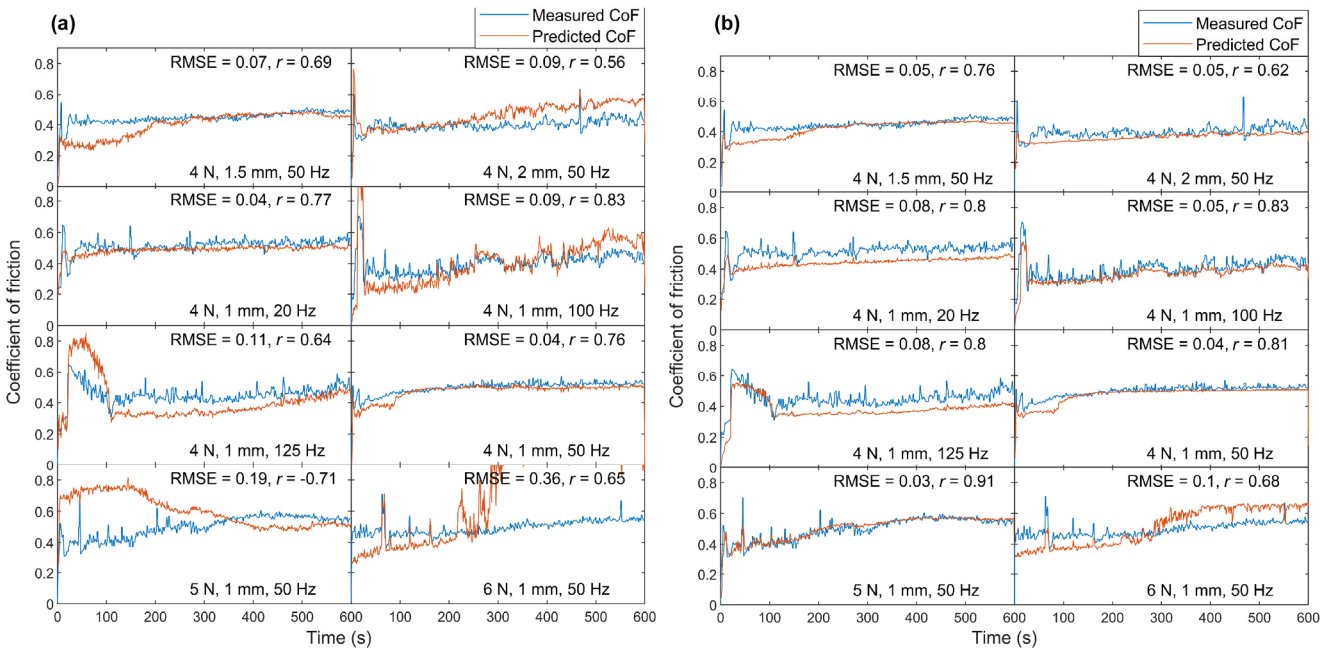

Fig. A1 Measured friction and predictions from all CSM ML models. (a) SVM STFT, (b) GPR STFT, (c) SVM STHG, (d) GPR STHG, (e) SVM Down sampling, (f) GPR Down sampling, (g) SVM Trimmed AE, (h) GPR Trimmed AE, (i) SVM RMS, (j) GPR RMS.

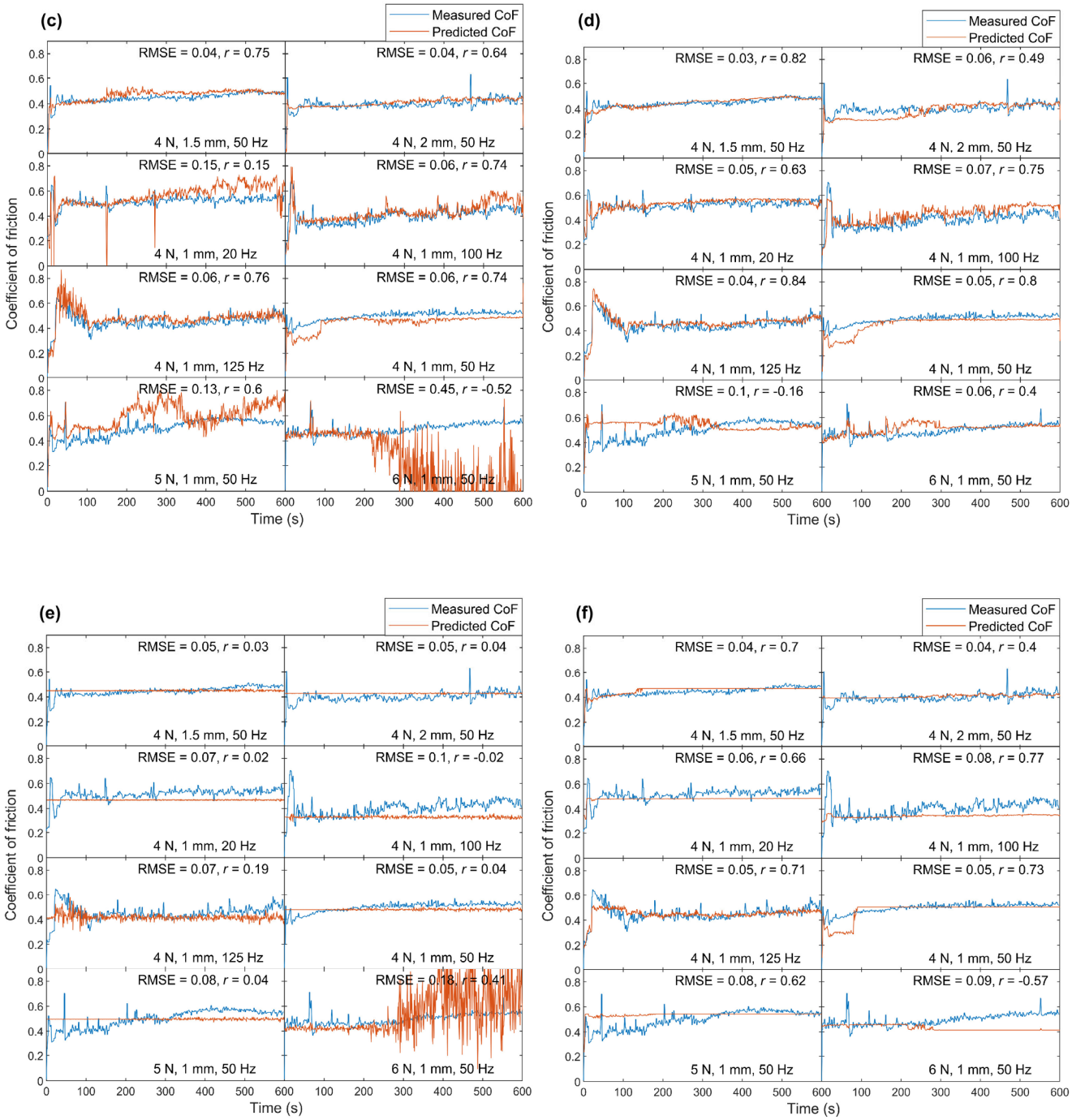

Fig. A1 (Continued)

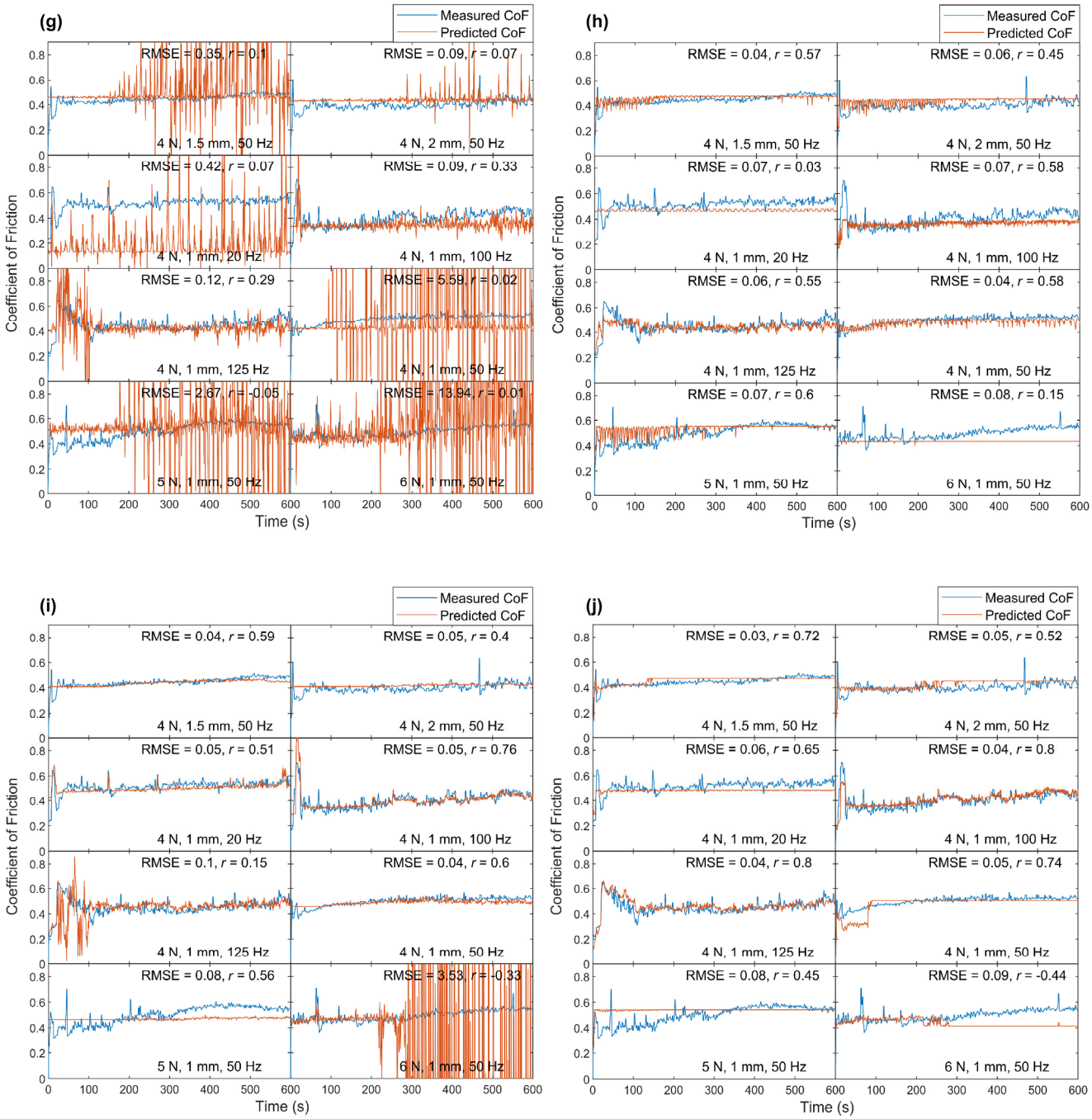

Fig. A1 (Continued)

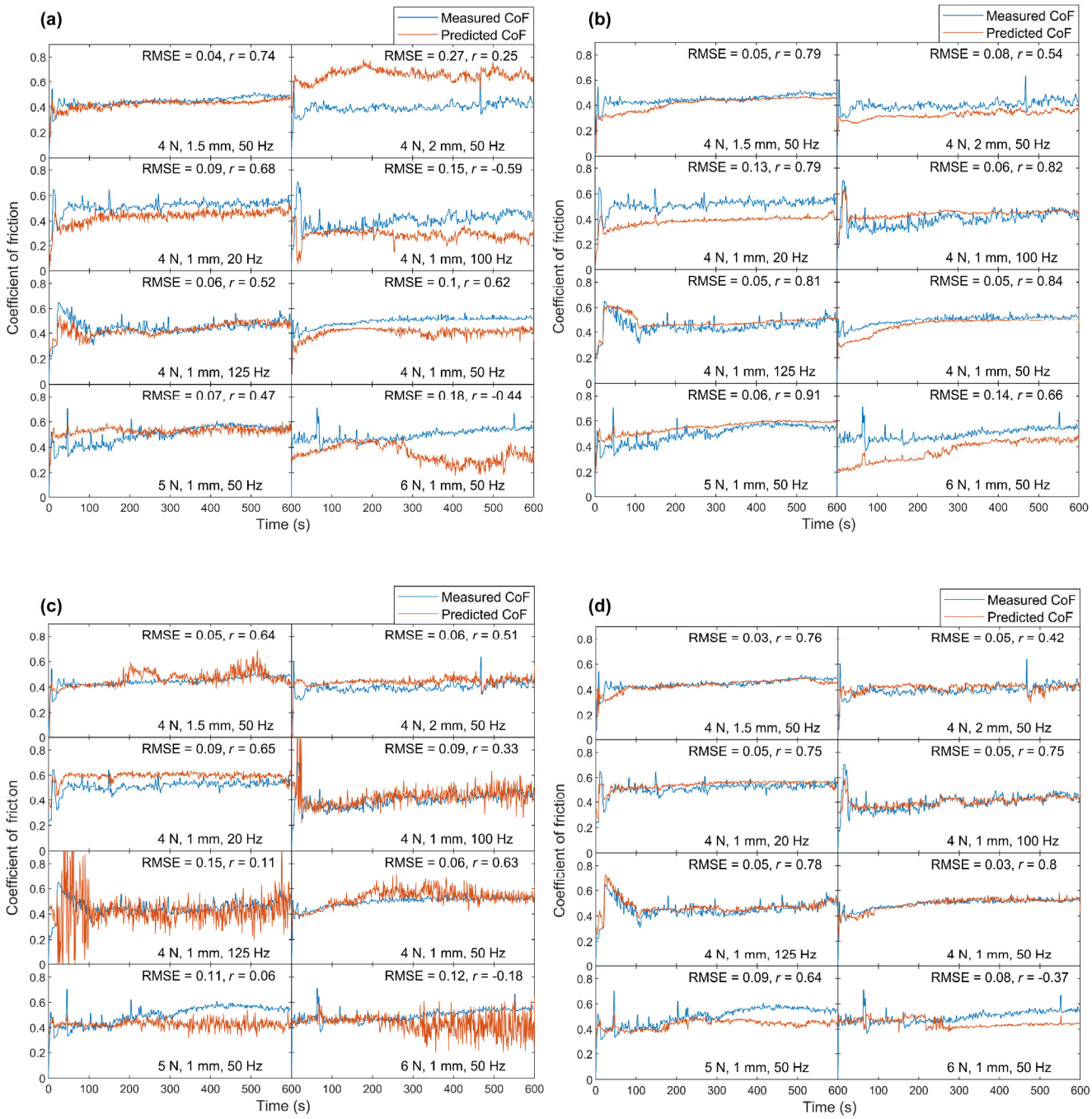

Fig. A2 Measured friction and predictions from all CGM ML models. (a) SVM STFT, (b) GPR STFT, (c) SVM STHG, (d) GPR STHG, (e) SVM Down sampling, (f) GPR Down sampling, (g) SVM Trimmed AE, (h) GPR Trimmed AE, (i) SVM RMS, (j) GPR RMS.

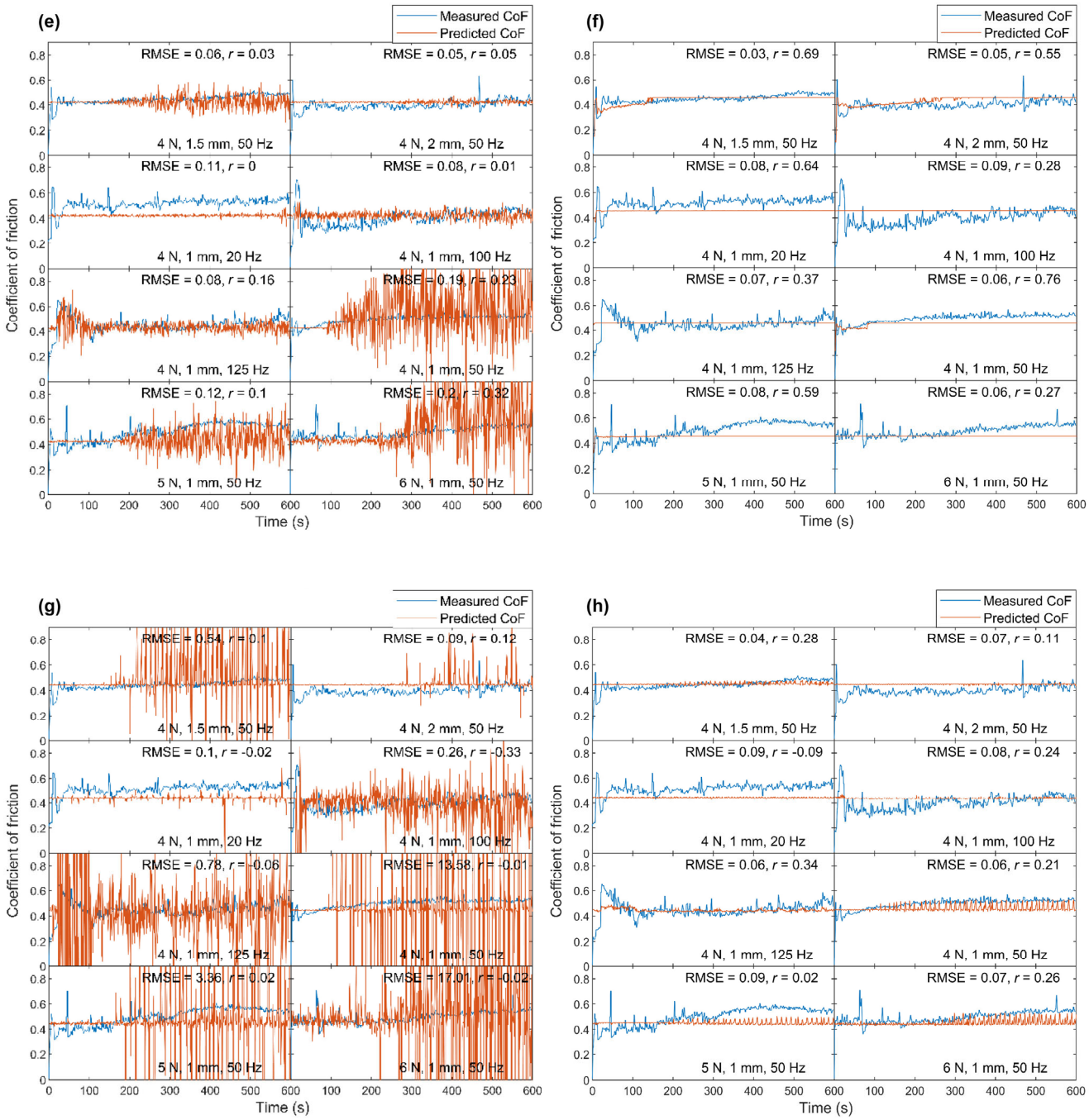

Fig. A2 (Continued)

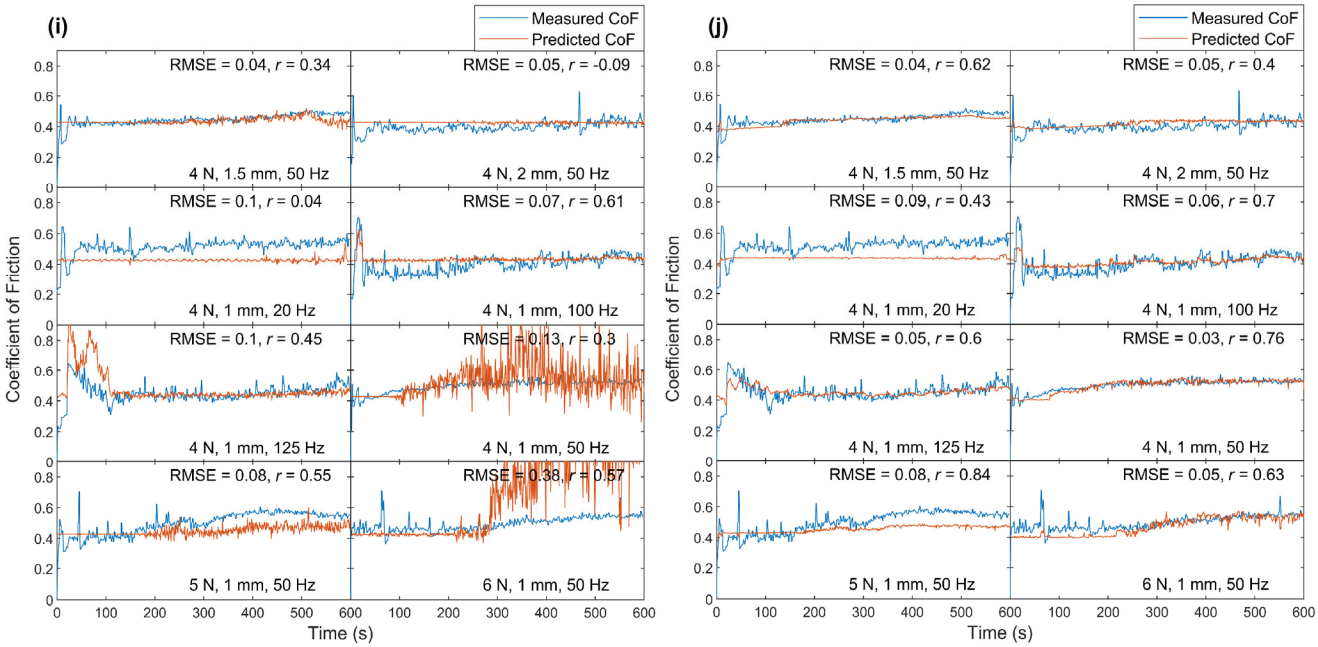

Fig. A2 (Continued)

References

[1] Holmberg K, Erdemir A. Influence of tribology on global energy consumption, costs and emissions. *Friction* **5**(3): 263–284 (2017)

[2] Holmberg K, Kivikytö-Reponen P, Härkisaari P, Valtonen K, Erdemir A. Global energy consumption due to friction and wear in the mining industry. *Tribol Int* **115**: 116–139 (2017)

[3] Anonymous, Machine Condition Monitoring Market by Monitoring Technique (Vibration Monitoring, Thermography, Oil Analysis, Corrosion Monitoring, Ultrasound Emission), Monitoring Process (Online, Portable), Deployment, Offering - Global Forecast to 2027. In *MarketsandMarkets*, 2022.

[4] Anonymous, Oil Condition Monitoring Market by Product Type (Turbines, Compressors, Engines, Gear Systems, Hydraulic Systems), Sampling Type, Vertical (Transportation, Industrial, Oil & Gas), and Region (2021-2026). In *MarketsandMarkets*, 2021.

[5] Mazal P, Dvoracek J, Pazdera L. Application of acoustic emission method in contact damage identification. *Int J Mater Prod Technol* **41**(1/2/3/4): 140 (2011)

[6] Feng P P, Borghesani P, Smith W A, Randall R B, Peng Z X. A review on the relationships between acoustic emission, friction and wear in mechanical systems. *Appl Mech Rev* **72**(2): 020801 (2020)

[7] Zhang X, Wang K W, Wang Y, Shen Y, Hu H S. Rail crack detection using acoustic emission technique by joint optimization noise clustering and time window feature detection. *Appl Acoust* **160**: 107141 (2020)

[8] Bol'shakov A M, Andreev Y M. Acoustic-emission testing of vertical steel tanks in hard-to-reach areas of the far north. *Russ J Nondestruct Test* **55**(3): 181–184 (2019)

[9] Crivelli D, McCrory J, Miccoli S, Pullin R, Clarke A. Gear tooth root fatigue test monitoring with continuous acoustic emission: Advanced signal processing techniques for detection of incipient failure. *Struct Health Monit* **17**(3): 423–433 (2018)

[10] Liu Z, Peng Q, He C, Wu B. Time difference mapping method for acoustic emission source location of composite plates. *ACTA ACUSTICA* **45**(3): 385–393 (2020) (in Chinese).

[11] Chernov D V, Matyunin V M, Barat V A, Marchenkov A Y, Elizarov S V. Investigation of acoustic emission in low-carbon steels during development of fatigue cracks. *Russ J Nondestruct Test* **54**(9): 638–647 (2018)

[12] Krampikowska A, Pała R, Dzioba I, Świt G. The use of the acoustic emission method to identify crack growth in 40CrMo steel. *Materials* **12**(13): 2140 (2019)

[13] Nivesrangsan P, Steel J A, Reuben R L. Source location of acoustic emission in diesel engines. *Mech Syst Signal Process* **21**(2): 1103–1114 (2007)

[14] Sun J, Wood R J K, Wang L, Care I, Powrie H E G. Wear monitoring of bearing steel using electrostatic and acoustic emission techniques. *Wear* **259**(7–12): 1482–1489 (2005)

[15] Miettinen J, Siekkinen V. Acoustic emission in monitoring sliding contact behaviour. *Wear* **181–183**: 897–900 (1995)

[16] Lingard S, Ng K K. An investigation of acoustic emission in sliding friction and wear of metals. *Wear* **130**(2): 367–379 (1989)

[17] Boness R J, McBride S L, Sobczyk M. Wear studies using acoustic emission techniques. *Tribol Int* **23**(5): 291–295 (1990)

[18] Mussa A, Krakhmalev P, Bergström J. Sliding wear and fatigue cracking damage mechanisms in reciprocal and unidirectional sliding of high-strength steels in dry contact. *Wear* **444–445**: 203119 (2020)

[19] Chevallier E. Mechanical model of the electrical response from a ring–wire sliding contact. *Tribol Trans* **63**(2): 215–221 (2020)

[20] Yang H J, Hu Y, Chen G X, Zhang W H, Wu G N. Correlation between the wear and vibration of the contact strip in a contact wire rubbing against a contact strip with electrical current. *Tribol Trans* **57**(1): 86–93 (2014)

[21] Jiaa C L, Dornfeld D A. Experimental studies of sliding friction and wear via acoustic emission signal analysis. *Wear* **139**(2): 403–424 (1990)

[22] Fan Y B, Gu F S, Ball A. Modelling acoustic emissions generated by sliding friction. *Wear* **268**(5–6): 811–815 (2010)

[23] Hu S T, Huang W F, Shi X, Peng Z K, Liu X F, Wang Y M. Bi-Gaussian stratified effect of rough surfaces on acoustic emission under a dry sliding friction. *Tribol Int* **119**: 308–315 (2018)

[24] Towsyfyan H, Gu F S, Ball A D, Liang B. Modelling acoustic emissions generated by tribological behaviour of mechanical seals for condition monitoring and fault detection. *Tribol Int* **125**: 46–58 (2018)

[25] Fuentes R, Dwyer-Joyce R S, Marshall M B, Wheals J, Cross E J. Detection of sub-surface damage in wind turbine bearings using acoustic emissions and probabilistic modelling. *Renew Energy* **147**: 776–797 (2020)

[26] Suzuki H, Kinjo T, Hayashi Y, Takemoto M, Ono K, Hayashi Y. Wavelet transform of acoustic emission signals. *J Acoust Emiss* **14**(2): 69–84 (1996)

[27] Geng Z, Puhan D, Reddyhoff T. Using acoustic emission to characterize friction and wear in dry sliding steel contacts. *Tribol Int* **134**: 394–407 (2019)

[28] Strablegg C, Renhart P, Summer F, Grün F. Methodology, validation & signal processing of acoustic emissions for selected lubricated tribological contacts. *Mater Today Proc* **62**: 2604–2610 (2022)

[29] Baccar D, Söffker D. Wear detection by means of wavelet-based acoustic emission analysis. *Mech Syst Signal Process* **60–61**: 198–207 (2015)

[30] Hase A, Mishina H, Wada M. Correlation between features of acoustic emission signals and mechanical wear mechanisms. *Wear* **292–293**: 144–150 (2012)

[31] Fuentes R, Howard T P, Marshall M B, Cross E J, Dwyer-Joyce R S. Observations on acoustic emissions from a line contact compressed into the plastic region. *Proc Inst Mech Eng Part J J Eng Tribol* **230**(11): 1371–1376 (2016)

[32] König F, Sous C, Ouald Chaib A, Jacobs G. Machine learning based anomaly detection and classification of acoustic emission events for wear monitoring in sliding bearing systems. *Tribol Int* **155**: 106811 (2021)

[33] Sattari Baboukani B, Ye Z J, G Reyes K, Nalam P C. Prediction of nanoscale friction for two-dimensional materials using a machine learning approach. *Tribol Lett* **68**(2): 57 (2020)

[34] Hasan M S, Kordijazi A, Rohatgi P K, Nosonovsky M. Triboinformatic modeling of dry friction and wear of aluminum base alloys using machine learning algorithms. *Tribol Int* **161**: 107065 (2021)

[35] Strablegg C, Summer F, Renhart P, Grün F. Prediction of friction power via machine learning of acoustic emissions from a ring-on-disc rotary tribometer. *Lubricants* **11**(2): 37 (2023)

[36] Rastegaev I A, Merson D L, Danyuk A V, Afanasyev M A, Vinogradov A. Using acoustic emission signal categorization for reconstruction of wear development timeline in tribosystems: Case studies and application examples. *Wear* **410–411**: 83–92 (2018)

[37] Benabdallah H S, Aguilar D A. Acoustic emission and its relationship with friction and wear for sliding contact. *Tribol Trans* **51**(6): 738–747 (2008)

[38] Hanchi J, Klamecki B E. Acoustic emission monitoring of the wear process. *Wear* **145**(1): 1–27 (1991)

[39] Braga-Neto U. Fundamentals of Pattern Recognition and Machine Learning. Cham: Springer International Publishing, (2020).

[40] Stalph P. *Analysis and Design of Machine Learning Techniques: Evolutionary Solutions for Regression, Prediction, and Control Problems.* Wiesbaden: Springer Fachmedien Wiesbaden, (2014).

[41] Rasmussen C, Nickisch H. *Gaussian Processes for Machine Learning.* MIT Press, 2005.

[42] Drezet P, Harrison RF. Directly optimised support vector machines for classification and regression. ACSE Research Report 715, The University of Sheffield (1998)

[43] Friel T, Harrison R. Linear programming support vector machines for pattern classification and regression estimation and the SR Algorithm: Improving speed and tightness of VC bounds in SV algorithms. In *ACSE Research Report 706*, Sheffield, UK, 1998

[44] Weiss J, Richeton T, Louchet F, Chmelik F, Dobron P, Entemeyer D, Lebyodkin M, Lebedkina T, Fressengeas C, McDonald R J. Evidence for universal intermittent crystal plasticity from acoustic emission and high-resolution extensometry experiments. *Phys Rev B* **76**(22): 224110 (2007)

[45] Miguel M C, Vespignani A, Zapperi S, Weiss J, Grasso J R. Intermittent dislocation flow in viscoplastic deformation. *Nature* **410**(6829): 667–671 (2001)

[46] Richeton T, Dobron P, Chmelik F, Weiss J, Louchet F. On the critical character of plasticity in metallic single crystals. *Mater Sci Eng A* **424**(1–2): 190–195 (2006)

[47] Bougherira Y, Entemeyer D, Fressengeas C, Kobelev N P, Lebedkina T A, Lebyodkin M A. The intermittency of plasticity in an Al3%Mg alloy. *J Phys*: *Conf Ser* **240**: 012009 (2010)

[48] Lebyodkin M A, Kobelev N P, Bougherira Y, Entemeyer D, Fressengeas C, Gornakov V S, Lebedkina T A, Shashkov I V. On the similarity of plastic flow processes during smooth and jerky flow: Statistical analysis. *Acta Mater* **60**(9): 3729–3740 (2012)

[49] Lebyodkin M A, Shashkov I V, Lebedkina T A, Mathis K, Dobron P, Chmelik F. Role of superposition of dislocation avalanches in the statistics of acoustic emission during plastic deformation. *Phys Rev E* **88**(4): 042402 (2013)

[50] Merchant M E. *The Friction and Lubrication of Solids*. Bowden F P and Tabor D. New York: Oxford Univ. Press, 1950. 337 pp. $7.00. *Science* **113**(2938): 443–444 (1951)

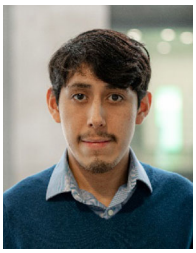

Robert GUTIERREZ. He is currently a Ph.D. student in the Department of Mechanical Engineering, Imperial College London. He completed his master's degree in 2020 also at the Department of Mechanical Engineering, Imperial College London. His research is focused on developing acoustic emission techniques for monitoring rubbing contacts.

Tianshi FANG. He is a Project Leader and Researcher at Shell Lubricants Technology since 2019. He has been working on multiple projects related to computational simulation, theoretical analysis, mathematical modeling, and experimental test of lubricants and coolants. He is a mechanical engineer by education. He obtained his Bachelor's degree with First Class Honours from the University of Hong Kong in 2012, and his Master's and Ph.D. degrees from Massachusetts Institute of Technology in 2014 and 2019. His research in graduate school was focused on the computational simulations and modeling of lubricating oil flow in piston-ring systems in automotive engines.

Robert MAINWARING. He studied mechanical engineering at Loughborough University in the UK. After graduation, he was employed by Mirrlees Blackstone Diesels Ltd. as a development engineer responsible for enhancing the efficiency of their 400 mm bore K Major diesel engine. A three year spell with the UK's National Nuclear Corporation focused on computational fluid dynamics followed. He was recruited by Shell in 1988 to research links between lubricants, engines and particulate emissions. Later roles have included lubricant additive research and Industry committee liaison, underpinning his current roles of Technology Manager for Innovation and Senior Principal Scientist within Shell's Lubricants Technology group, where he leads a wide range of projects targeted at enhancing, demonstrating and communicating the role of lubricants in the performance of engineering equipment.

Tom REDDYHOFF. He is a reader (~associate professor) in the Department of Mechanical Engineering, Imperial College London. His research focuses on improving the performance of sliding contacts and often involves developing novel *in situ* measurement techniques used in combination with numerical modelling.